Sr, Nd and Pb isotope constraints on the formation of the metalliferous sediments in the Nereus Deep, Red Sea

Delphine Bosch [a], Joël Lancelot [a], Jacques Boulegue [b]

[a] *Laboratoire de Géochronologie–Géochimie–Petrologie, C.N.R.S.U.R.A. 1763, Departement S.T.U., U.M.II, Case courrier 066, 34095 Montpellier Cedex 05, France*

[b] *Laboratoire de Géochimie et Métallogénie, C.N.R.S.U.R.A 196, Université Pierre et Marie Curie, 4 place Jussieu, F-75230 Paris Cedex 05, France*

(Received March 16, 1993; revision accepted March 15, 1994)

Abstract

Previous chemical analyses of sediments from Nereus Deep core 412, located in the northern part of the Red Sea at about 23°20′N, have demonstrated the occurrence of V-rich authigenic magnetites associated with Fe, Zn and Cu sulphides mostly located at the bottom of the core. The evolutionary stage of Nereus Deep is intermediate between that of the immature Shaban Deep and the more evolved Atlantis II Deep. Previous studies have proposed either MORB basalts (by analogy with East Pacific Rise sulphide deposits) or sediments as possible sources of the metals in the Red Sea metalliferous sediments. Sr, Nd and Pb isotope systematics, observed at ten levels in Nereus core 412, lead us to distinguish three types of sediments, (1) with predominantly basaltic fragments associated with loose titanomagnetite crystals ($0.70413 \leqslant {}^{87}Sr/{}^{86}Sr \leqslant 0.70622$; $0.51271 \leqslant {}^{143}Nd/{}^{144}Nd \leqslant 0.51300$; $18.618 \leqslant {}^{206}Pb/{}^{204}Pb \leqslant 18.673$), (2) detrital or biogenic sediments with a continental isotopic imprint ($0.70938 \leqslant {}^{87}Sr/{}^{86}Sr \leqslant 0.71323$; $0.51242 \leqslant {}^{143}Nd/{}^{144}Nd \leqslant 0.51262$; $18.848 \leqslant {}^{206}Pb/{}^{204}Pb \leqslant 18.890$), and (3) V-rich metalliferous sediments ($0.70872 \leqslant {}^{87}Sr/{}^{86}Sr \leqslant 0.70895$; $0.51260 \leqslant {}^{143}Nd/{}^{144}Nd \leqslant 0.51274$; $18.717 \leqslant {}^{206}Pb/{}^{204}Pb \leqslant 18.851$). On Sr-Nd and Pb-Pb isotope diagrams this last group of sediments defines a field located between the fields of the first two groups. Our data suggest that the Sr, Nd and Pb in the studied metalliferous sediments were derived from overlying sedimentary beds in which the two main constituent detrital components show very distinct origins (Red Sea MORB and continental Arabo-Nubian Shield). These data clearly support a model of convective circulation within the Nereus Deep sedimentary pile. This model involves leaching two main components from the upper sedimentary layers of the core and a downward circulation of a hot fluid promoting the growth of V-rich magnetites and Fe, Zn and Cu sulphides when the fluid cooled by mixing with the pore water of sediments from the lower part of the core. A driving force, represented by magmatic activity located near the 412 core in the Nereus Deep, is required to explain the presence of hot convective fluids. These data also suggest that, for sedimented ridges, the isotopic imprint of a basaltic source in metalliferous sediments or a hydrothermal ore deposit may result by interaction of a hot fluid with detrital sediments that are enriched in basaltic clasts and loose magmatic crystals.

1. Introduction

In recent years, much attention has focused on deep-sea metalliferous brines and deposits. Critical questions have been raised: What is the origin and mode of concentration of the metals? What is the economic significance of oceanic hydrothermal deposits and of the models of their formation? Are there applications to the origin of ancient ore bodies? The concept of 'metalliferous sediments' appears in studies by Börstrom and Peterson [1], who describe Fe- and Mn-rich sediments on the East Pacific Rise (EPR) expressed as oxyhydroxides with a low Al content.

Metalliferous oceanic hydrothermal deposits were first discovered on the Galapagos Ridge by Corliss et al. [2]. Although initially thought to be restricted to mid-ocean ridges such as the EPR [3–9], the Mid-Atlantic Ridge (MAR) [10–12] and the Red Sea [13,14] hot or cold spring deposits have been discovered recently in variously sedimented ridges of back-arc basins such as the Marianas [15], Okinawa [16] North Fiji [17,18] and Lau [19]. Recent seafloor sulphide deposits on the EPR have Pb isotopic compositions similar to those of the surrounding tholeiitic basalts, which suggests that mineralizing fluids acquired some chemical and isotopic characteristics by high-temperature interaction with a MORB component [7,9,20,21]; meanwhile $\delta^{18}O$, ϵ_{Sr} and $\delta^{34}S$ values differ from those found in oceanic basalts and indicate a mixing process between hydrothermal fluid and seawater [22,23].

The conditions of hydrothermal feeding of the hot brine pools in the Red Sea are still controversial because, in the case of sedimented ridges, models of sulphide ore formation must take into account possible contributions from various sedimentary components. Recent studies have emphasized that, in various geodynamic contexts, the presence of ore deposits of economic interest (with galena, amorphous silica and barite associated) is related to important continental sediment influxes. This continental contribution is observed on some mid-oceanic ridges (Escabana Trough [9]) and in some back-arc basins (Okinawa [16] and Lau [19]).

The Red Sea is a recent oceanic zone [24–27]. Large sediment accumulations consisting of very thick (5–6 km) salt deposits of Middle–Late Miocene age are observed in this area. The nature of the crust below these Miocene evaporites and the initiation times of oceanic opening are still a matter of vigorous debate [28]. Continuous oceanic crust is present in the southern Red Sea (16–20°N) today and has been dated by magnetic anomalies at between 5 and 6 Ma [29]. To the northwest, the oceanic crust becomes progressively younger and the axial deeps are more isolated and narrower. Thus, the central segment of the Red Sea is characterized by about fifteen axial deeps (Figs. 1 and 2) ranging from several kilometres to less than one kilometre in length, most of them containing hot and cold brines associated with metalliferous sediments [30].

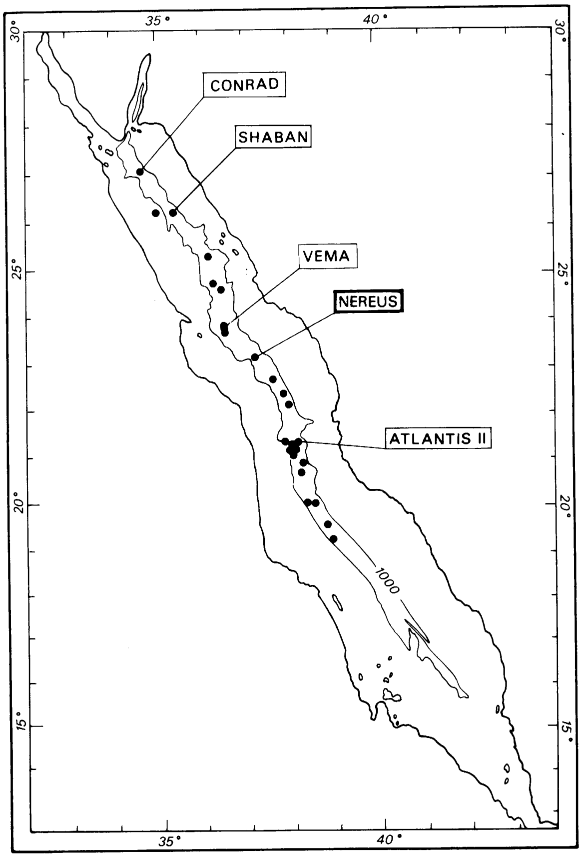

Fig. 1. Sketch map of the Red Sea with locations of the main deeps after Pautot et al. [30].

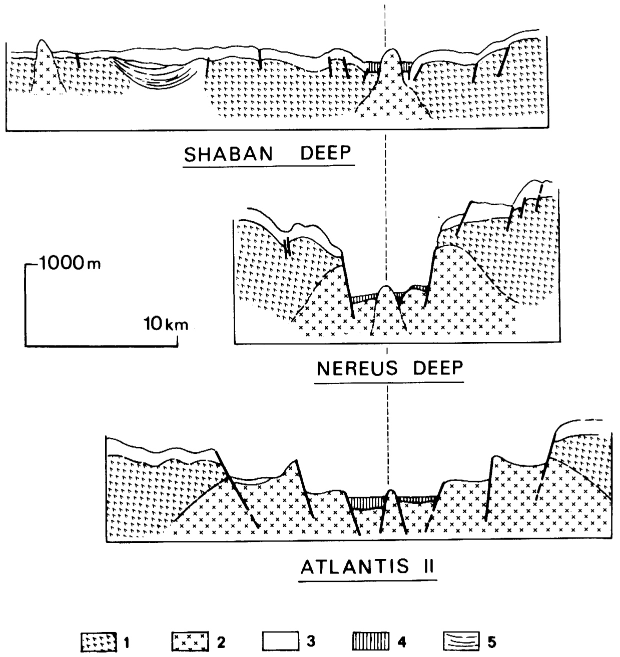

Fig. 2. Interpreted seismic profiles from the Red Sea deeps (modified after [43]) illustrating the three main evolutionary stages: immature (e.g., Shaban Deep), intermediate (e.g., Nereus Deep) and evolved (e.g., Atlantis II Deep). *1* = Miocene evaporites; *2* = basalts; *3* = recent sediments; *4* = brines; *5* = lateral depressions.

Among the numerous Red Sea Deeps (Fig. 1), Atlantis II is the largest and most studied, because of its famous Zn, Cu, Ag and Au-rich sediments [31–35].

In spite of numerous investigations, the origin of hydrothermal salt brine pools in the Red Sea deeps is still a matter of debate. Shanks and Bishoff [36] suggested that the most likely source of the sulphides results from the reduction of a small amount of brine sulphates which have interacted with ferrous minerals from rift basalts. Another hypothesis, suggested by Kaplan et al. [37], implies a participation of shales enriched in organic matter. The first Pb isotope measurements of Red Sea metalliferous sediments [38] and He isotope measurements of the Red Sea brines [13] indicated a basaltic component. Carbon isotope compositions of the Atlantis II brines did not indicate reaction with organic matter [39]. However, on the basis of new Pb isotope data, Dupré et al. [35] have proposed that metals concentrated in the Atlantis II Deep sediments were not derived from a basaltic source but were provided by recent biogenic terrigenous sediments and another, unknown, sedimentary source. In contrast, Calvez et al. [40] on the basis of Sr, Nd, Pb and REE data from sediments from various Red Sea deeps, suggested that hydrothermal fluids interacted with rift basalts to explain the isotopic characteristics of the metalliferous sediments.

The purpose of this paper is to constrain the processes leading to the accumulation of metalliferous sediments in the Red Sea on the basis of new isotope data obtained from Nereus Deep samples (Fig. 1). We have carried out an expanded geochemical study using various isotopic tracers (Rb/Sr, Sm/Nd and U/Th/Pb) to distinguish the interactions between hydrothermal fluids and various sedimentary components recognized within the studied Nereus Deep core (detrital terrigenous and biogenic sediments, basaltic fragments, loose titanomagnetite crystals, and hematite and sulphide-rich layers). A petrographic study and EDS/EMP chemical analyses have already performed on the same samples from this Nereus Deep drillcore [41]. The identification of metal sources for the Nereus Deep metalliferous sediments involves the use of several geochemical tracers, because for this nascent sedimented ridge the isotopic imprint of both crustal rocks of the Arabo-Nubian Shield and mantle-derived Red Sea MORB should be expressed in its sediments.

2. Geological background

The Nereus Deep is located north of the Atlantis II Deep, at around 23°2′N in the axial zone of the Red Sea (Fig. 1). The Nereus Deep structure is essentially composed of a large graben that is about 30 km long and 10 km wide. Oceanic crust outcrops at lower levels. Miocene evaporites and Plio-Quaternary sediments overlie the oceanic crust, especially on the northern edge of the deep. Guennoc et al. [42] inferred a four-stage evolution for the Nereus Deep, which should be less than 1 Ma old: (1) A narrow axial trough, which could have been produced by collapse-type deformation as a consequence of the rupture of evaporite layers under extensional stress, (2) axial deep and shallow intraevaporitic axial intrusions (Vema and Conrad stage, Figs. 1 and 2), (3) first appearance of a volcanic seamount, beginning of graben formation, and collapse of volcanic basement (Shaban Deep stage, Figs. 1 and 2), and (4) increased axial volcanic activity and building of a small volcanic ridge in the graben (Nereus Deep stage, Figs. 1 and 2). In fact, the Nereus Deep exhibits an intermediate evolutionary stage between those of the northern, more immature Shaban Deep and the more evolved southern Atlantis II Deep. Guennoc et al. [42] suggested that with increased magmatism a larger volcanic edifice could form and the future structure of the northern part of this deep could then be one of a large axial volcanic seamount separating two deep basins bounded by scarps on which basaltic basement and evaporites would outcrop. These types of axial valley stuctures reflect the processes controlling ocean opening at very slow spreading rates [43].

3. The studied samples

Nereus Deep core 412 was collected in September 1981 by crews from the *Laboratoire de Géologie Marine du Muséum d'Histoire Naturelle* and the *Laboratoire d'Océanologie et Géodynamique de l'Université de Brest* aboard the R.V. *Marion Dufresne*. Chemical study of this core (EMP and EDS) [41] led to the discovery of high vanadium concentrations in authigenic magnetites and vanadomagnetites (up to 1.3% V_2O_3) in several samples. The low content or absence of titanium in these authigenic iron minerals was surprising, because it is well known that the occurrence of vanadium in magnetite and hematite from high-temperature iron deposits is always related to greater or at least equal quantities of titanium [41]. The core was divided into two zones (Fig. 3):

The upper zone, I (0–107 cm), is characterized by biogenic carbonate beds with variable contents of Fe and Mn oxyhydroxides. Four samples (1, 2, 9 and 3) from this zone were studied:

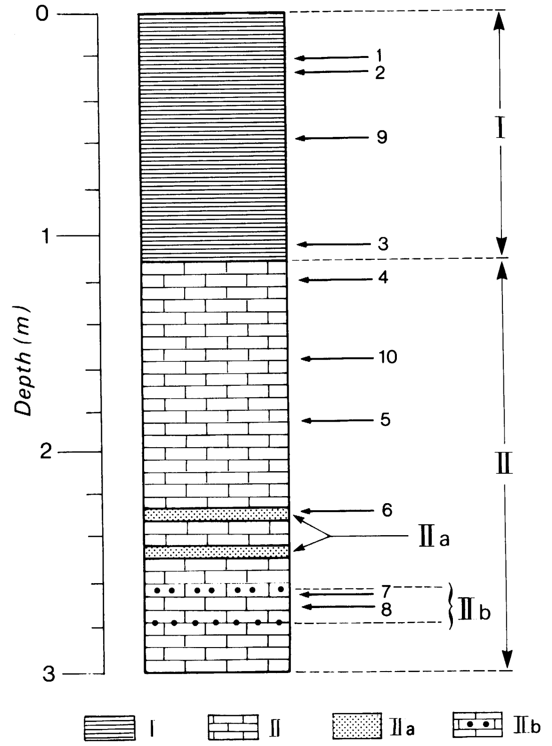

Fig. 3. Sediment sequence in Nereus Deep core 412, with location of studied samples (1–10) (after Jedwab et al. [41]). *I* = alternating beds of biogenic carbonates with varying amounts of oxyhydroxides; *II* = carbonate muds with oxides; *IIa* = hematite and sulphide-rich beds; *IIb* = sulphide-rich beds.

(1) (22–23 cm): Yellowish brown mud, with basaltic fragments and loose titanomagnetite crystals.
(2) (27–28 cm): Brown heterogeneous sample with carbonaceous deep-sea organisms, basaltic fragments and loose titanomagnetite crystals. On the basis of chemical and mineralogical analysis [49], these basaltic fragments are similar to tholeiitic basalts that outcrop on the axis of the Red Sea. The major elements identified in this sample are MgO, Al_2O_3, SiO_2, CaO and FeO, with contents of 5.5%, 8.0%, 35.3%, 21.4% and 35.5% respectively [41].
(9) (56–57 cm): Brown mud with numerous biogenic carbonate crystals and Mn oxides.

(3) (106 cm): Orange to red hematite-rich mud with an FeO content of about 84.1%.

Samples 1 and 2 show a noticeable amount of basaltic rock fragments (more than 5% with a size of a few millimetres). Jedwab et al. [41] proposed that the high V-content of the authigenic vanadomagnetites is a consequence of hydrothermal leaching of Fe-Ti oxides, which are abundant (as loose crystals and in basaltic clasts) in the sediments of the upper part of the core.

The lower zone, II (107–300 cm), is predominantly carbonate mud with various oxides. The main components are smectite, biogenic carbonates, hematite and Mg-rich calcite; locally magnetite and various oxyhydroxides are observed. Zone II includes two peculiar units, called IIa and IIb. Unit IIa comprises two hematite-rich beds located at 222–227 cm and 243–248 cm in core 412. Unit IIb includes two sulphide-rich beds (pyrite, sphalerite and chalcopyrite associated with vanadomagnetite) located at the 268–284 cm level.

Six samples (4, 5, 6, 7, 8 and 10) from this zone were studied:

(4) (119 cm): Grey mud of a granular texture with abundant altered basaltic fragments and loose titanomagnetite crystals. These rock fragments are rounded and cavernous, but still display the typical hypautomorphic–granular or devritification textures of mafic rocks which have been collected in Red Sea dredgings and outcrops [41]. MgO, SiO_2, CaO and FeO are the main constituents of this sample, with amounts of 5.2%, 22.5%, 40.4% and 25.8% respectively [41].

(10) (156–157 cm): Brown chalk with detrital biogenic carbonates and smectites.

(5) (185–186 cm): Brown mud with abundant vanadomagnetites and Fe, Cu and Zn sulphides.

(6) (224–225 cm): Brown-red hematite-rich mud with a very low V content and high FeO content (> 96%).

(7) (268–269 cm): Dark green mud, with very high amounts of Fe, Cu and Zn sulphides and vanadomagnetites. This sample constitutes, with samples 5 and 8, one of the V-rich sediments.

(8) (271–272 cm): Black mud, one of the most V-rich sediments.

4. Analytical methods

Ten samples of Nereus Deep core 412 were analyzed to define the isotopic variability of the sediments. All the analyzed samples were desalted several times by ultrasonifying in distilled water for a few hours. Extended and repeated cycles of centrifuging ensured that the samples were well rinsed. After ten steps of rinsing and centrifuging no remaining seawater influence was detected. The Sr content of waters obtained after the last step of centrifuging falls in the range of the total Sr blank.

The chemical and mass spectrometry procedures have been described already [25,44,45], and are only briefly reviewed here: The water-insoluble fraction was digested in a Teflon bomb with a mixture of triple distilled 13*N* HNO_3 and 48% HF with a few drops of $HClO_4$. Two aliquots were separated, one for the determination of Pb, Sr and Nd isotopic compositions and the other for Pb, U, Th, Sr, Rb, Nd and Sm contents. Concentrations were measured by isotope dilution using ^{206}Pb-^{235}U-^{232}Th, ^{84}Sr-^{87}Rb and ^{146}Nd-^{149}Sm mixed spikes.

Considering the heterogeneity of the various sedimentary components of the Nereus core, leaching experiments were conducted in order to preferentially remove altered components and carbonates. Thus, three Sr isotope compositions were measured for each sample. These correspond to the salt-free samples, the solutions recovered from acid-leaching steps and the final solid residues. Leaching experiments were completed in 2.5*N* HCl for 15 min at room temperature, 5 min at 70°C and for 10 min in an ultrasonic tank. After leaching and centrifuging the leachates were evaporated to dryness and the solid residues were digested for 48 h in a mixture of 48% HF and 13*N* HNO_3 with a few drops of $HClO_4$.

The isotopic data were measured on a fully automated V.G. Sector mass spectrometer. To assess the reproducibility and accuracy of the Sr measurements, NBS 987 was repeatedly run (12 times) during this study, the average value being 0.710245 with a precision better than ± 0.000013 (2σ). $^{87}Sr/^{86}Sr$ ratios are corrected for mass discrimination by normalizing to a $^{86}Sr/^{88}Sr$ value of 0.1194. To assess the accuracy of the Nd composition measurements the JMC 361 standard was analyzed repeatedly (8 times), the average value being 0.511141 with an error of ± 0.000016 (2σ). $^{143}Nd/^{144}Nd$ ratios were normalized to a $^{146}Nd/^{144}Nd$ value of 0.7219. The Pb data were calibrated against measurements of NBS 981 with a mass discrimination factor of 0.0192 ± 0.0016 a.m.u. Sr, Nd and Pb total blank concentrations were less than 0.25, 0.18 and 0.09 ng respectively.

5. Results, and constraints on the formation of the metalliferous sediments

5.1. Sr isotopic compositions

The Sr isotopic compositions and Rb-Sr contents of sediments from Nereus Deep core 412 are reported in Table 1a. All Sr isotope compositions from the Nereus Deep are plotted versus

Table 1a
Sr isotopic composition (unleached samples, leachates and solid residues measured during the first leaching experiments) and Rb-Sr contents of salt-free sediments from Nereus Deep core 412. Errors are given at the 2σ level, normalization values are given in the analytical methods section. ϵ_{Sr} values were calculated following De Paolo and Wasserburg [44] using $^{87}Sr/^{86}Sr = 0.7045$ for present-day CHUR. In the four tables, dashes indicate not analyzed

Sample	Depth (cm)	Sr (ppm) unleached samples	Rb (ppm) unleached samples	$^{87}Sr/^{86}Sr$ unleached samples	$^{87}Sr/^{86}Sr$ leached phases	$^{87}Sr/^{86}Sr$ solid residues
1	22-23	85.3	0.68	0.70798±2 *εSr= +49*	0.70890±1 *εSr= +62*	0.70622±2 *εSr= +24*
2	27-28	157.6	0.62	0.70819±2 *εSr= +52*	0.70898±3 *εSr= +64*	0.70732±4 *εSr= +40*
9	56-57	336.0	–	0.70914±4 *εSr= +66*	0.70910±1 *εSr= +65*	–
3	106	31.9	0.39	0.70915±2 *εSr= +66*	0.70899±1 *εSr= +64*	0.70938±1 *εSr= +69*
4	119	102.8	0.72	0.70875±2 *εSr= +60*	0.70894±1 *εSr= +63*	0.70792±1 *εSr= +49*
10	156-157	171.1	3.81	0.70882±3 *εSr= +61*	0.70879±2 *εSr= +61*	0.70959±2 *εSr= +72*
5	185-186	61.4	0.22	0.70886±3 *εSr= +62*	0.70911±1 *εSr= +65*	0.70874±3 *εSr= +60*
6	224-225	22.7	0.15	0.70843±3 *εSr= +56*	0.70860±5 *εSr= +58*	0.70826±2 *εSr= +53*
7	268-269	127.9	0.73	0.70882±2 *εSr= +61*	–	0.70872±1 *εSr= +60*
8	271-272	2.3	0.96	0.70921±4 *εSr= +67*	–	0.70895±2 *εSr= +63*

Table 1b
Sr isotopic composition and Rb-Sr contents (leachates and solid residues measured after the second leaching experiments) of salt-free sediments from Nereus Deep core 412

Sample	Depth (cm)	Sr (ppm) solid residues	Rb (ppm) solid residues	$^{87}Sr/^{86}Sr$ solid residues	Sr (ppm) leached phases	Rb (ppm) leached phases	$^{87}Sr/^{86}Sr$ leached phases
2	27-28	60.9	0.3	0.70413±2 *εSr= -05*	697.0	5.2	0.70894±2 *εSr= +63*
9	56-57	10.5	2.2	0.70992±1 *εSr= +77*	1603.0	5.5	0.70918±2 *εSr= +66*
4	119	17.1	0.3	0.70540±1 *εSr= +13*	578.4	3.7	0.70893±4 *εSr= +63*
10	156-157	26.7	2.7	0.71323±1 *εSr= +124*	232.6	5.2	0.70883±2 *εSr= +61*

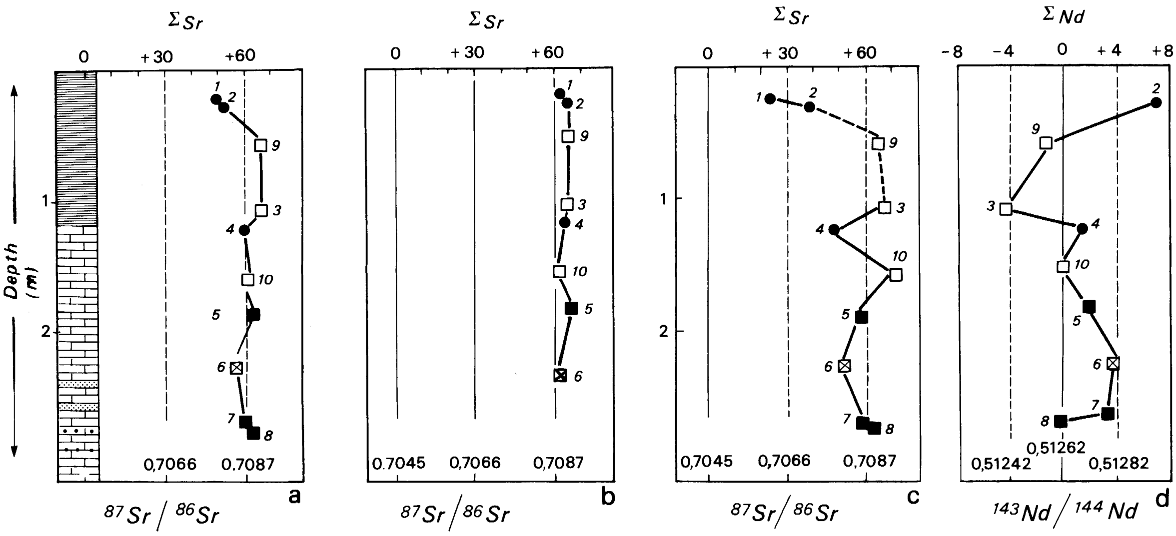

Fig. 4. Isotopic stratigraphy for Nereus Deep core 412. From left to right the columns represent profiles versus depth (m) of (a) $^{87}Sr/^{86}Sr$ ratio for desalted and unleached samples, (b) $^{87}Sr/^{86}Sr$ ratio for acid leaches, (c) $^{87}Sr/^{86}Sr$ ratio for solid residues after acid leaching, and (d) $^{143}Nd/^{144}Nd$ ratio for solid residues after acid leaching. ● = detrital sediments with basaltic fragments and loose titanomagnetite crystals (1, 2 and 4); □ = biogenic–terrigenous sediments (9, 3 and 10); ■ = V-rich metalliferous sediments (5, 7 and 8); ⊠ = hematite-rich sediment (6).

depth in Figs. 4a–c and 5. Unleached samples have $^{87}Sr/^{86}Sr$ ratios ranging from 0.70798 to 0.70921 (Fig. 4a). Sr compositions for acid leaches range from 0.70860 to 0.70911, values which are similar to or slightly lower than the present Red Sea seawater and Miocene evaporite Sr isotopic composition (i.e., ~ 0.7092 and ~ 0.7089 respectively [34]) (Fig. 4b). Sr isotopic effects of seawater alteration and the occurrence of carbonates are clearly expressed for these samples. In such samples, seawater Sr originates from the precipitation of carbonated phases and fluid-rock reactions. This fluid is interstitial seawater and/or hydrothermal fluids showing the Sr isotopic composition of seawater or the composition achieved by mixing between seawater and evaporites, after percolation within the Miocene formation.

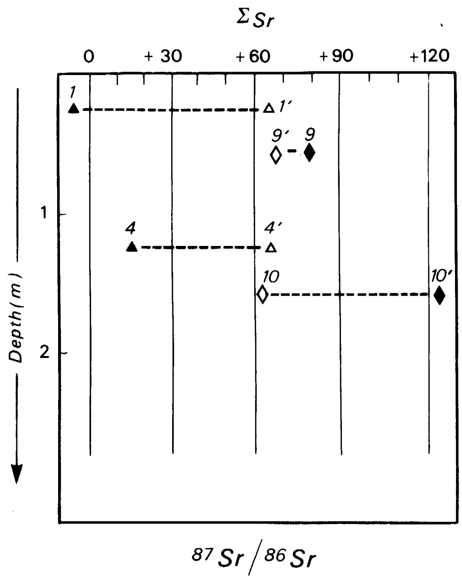

Fig. 5. $^{87}Sr/^{86}Sr$ ratios of solid residues (▲, ♦) and leachates (△, ◇) after experiments involving highly corrosive leaching.

Based on petrological data and the $^{87}Sr/^{86}Sr$ values of solid residues, we have distinguished three groups of samples in the sediments from Nereus Deep core 412 (Fig. 4c):

Samples 1, 2 and 4 form *group A*. These contain altered basaltic fragments and loose titanomagnetite crystals. Their solid residues show the lowest $^{87}Sr/^{86}Sr$ ratios, ranging from 0.70622 to 0.70792. The solid residue of sample 1 shows the least radiogenic $^{87}Sr/^{86}Sr$ ratio (0.70622) and the lowest Sr content (85.3 ppm) of the samples in this group; the $^{87}Sr/^{86}Sr$ ratio of this solid residue could indicate the Sr compositions of the basaltic components present in this group.

Samples 9, 3 and 10 form *group B*. The solid residues of these samples have the most radiogenic Sr isotope compositions, ranging from 0.70938 to 0.70959. These ratios are higher than those of the unleached samples and the present seawater Sr value of the Red Sea ($\sim$ 0.7092). This radiogenic character suggests the presence in these sediments of detrital terrigenous components equilibrated with Sr from continental crust (i.e., the neighbouring crust of the Arabo-Nubian Shield [46]).

Metalliferous sediments 5, 7 and 8 form *group C* and contain Fe, Cu and Zn sulphides and high V contents. The $^{87}Sr/^{86}Sr$ ratios of the solid residues of these samples ranges from 0.70872 to 0.70895, values intermediate between those of the two former groups.

Hematite-rich sample 6 has a very low V content, in spite of being interbedded with metalliferous sediments in the core (Figs. 3 and 4). The $^{87}Sr/^{86}Sr$ of its solid residue is 0.70826, a value lower than those of the group C sediments, but intermediate between values for sediments from groups A and B.

The Rb contents of Nereus Deep sediments are variable but usually low ($<$ 1 ppm), except for sample 10 (3.81 ppm). Sr contents are also scattered, with maximum values being obtained for two samples from group B (9 and 10) which have a large proportion of detrital components. In this group, sample 3 has the lowest Sr content, which could be explained by large amounts of hematite in this sample (as for sample 6). The different types of sediments identified above alternate at different levels in the sedimentary core. This reveals the extreme complexity of the sedimentation of this deep and suggests that the hydrothermal system implicated in the sedimentation of this deep is more likely to be discontinuous.

In a further attempt to constrain the initial Sr composition of the detrital components of sediments of groups A and B, additional leaching experiments involving highly corrosive methods were conducted on samples 2, 4, 9 and 10, using two attacks in 6*N* HCl for 30 min at 70°C, each time followed by 10 min in an ultrasonic tank. After centrifuging the leachates were evaporated to dryness and the solid residues were digested in a mixture of 13*N* HNO_3 and 48% HF for 48 h. The data are reported in Table 1b and plotted in Fig. 5. The $^{87}Sr/^{86}Sr$ ratios of the leachates are similar to those obtained during the first leaching experiments, with an average of 0.70895, which is very close to the Red Sea seawater and Miocene evaporites value, confirming extraction of seawater-like Sr, in agreement with the presence of biogenic carbonates in the four studied samples [41]. This does not demonstrate the complete removal of such carbonates, although the $^{87}Sr/^{86}Sr$ values obtained from the solid residues are clearly more radiogenic (samples 9 and 10), or less radiogenic (samples 2 and 4), than those obtained during the first leaching experiments. For the solid residues 9 and 10, $^{87}Sr/^{86}Sr$ values of 0.70992 and 0.71323 respectively are similar to Sr isotope values measured in rocks from the neighbouring Arabo-Nubian Shield (see [46] for references]. Solid residues 2 and 4 have $^{87}Sr/^{86}Sr$ ratios of 0.70413 and 0.70540 respectively. These ratios approach the Sr isotope values of the Nereus tholeiitic basalts, which range from 0.70289 to 0.70381 [47], in good agreement with the presence of basaltic clasts and loose titanomagnetite crystals in the group A sediments. The efficiency of the second acid leaching experiment in removing seawater-like Sr is confirmed by these data, even for Nereus Deep sediments for which the isotopic imprint of the detrital components is swamped by the seawater-like Sr of the biogenic carbonates. These detrital components exhibit two very disparate sources (continental crust of the Arabo-Nubian Shield for group B sediments (samples 9 and 10), and tholeiitic basalts of the Red Sea for group A sediments (samples 2 and 4)) which have been clearly identified by the $^{87}Sr/^{86}Sr$ ratios of the solid residues obtained after the most corrosive leachings.

5.2. Sm-Nd isotopes

Sm-Nd isotopic results are reported in Table 2 and ϵ_{Nd} values are plotted against depth in Fig. 4d. $^{143}Nd/^{144}Nd$ ratios range from 0.51300 to

0.51242. Plotted on the Sm/Nd diagram (Fig. 6a) these data define three separate fields corresponding to each group of sediments previously defined on the basis of Sr isotopic compositions. $^{147}Sm/^{144}Nd$ ratios for groups A, B and C range from 0.1515 to 0.1755, from 0.1048 to 0.1083 and from 0.0837 to 0.07925 respectively. In addition, group A has very low Sm and Nd contents (average 0.8 ppm for Nd and 0.23 ppm for Sm). Such low values are typical of tholeiites. In contrast, oceanic hydrothermal fluids are commonly enriched in LREE compared to seawater [48]. Metalliferous samples from Nereus Deep show a clear LREE enrichment expressed by low $^{147}Sm/^{144}Nd$ ratios.

The origin of this LREE enrichment can be considered in the light of the phosphorus chemistry in barren and metalliferous marine sediments. Phosphorus may be incorporated into metalliferous sediments by adsorption or coprecipitation from seawater, sedimentation of fish debris, or precipitation from hydrothermal solutions [49]. Positive correlations of ΣREE with P_2O_5 content and Zr/Hf ratio in the Atlantis II Deep sediments [33] have suggested that fish debris and finely crystallized apatite derived from the dissolution of such debris are major carriers of REE in marine sediments [50]. A microfossil distribution study of the Atlantis II Deep cores [51] has identified a correlation between the abundant supply of siliceous micro-organisms (radiolaria and diatoms) and fish debris with sulphide-rich beds. Thus, the record of animal life development, at specific stratigraphic levels in these Red Sea cores, has been related to sudden enrichment of seawater in silicon and nutrient elements by episodic discharges of geothermal brines rather than by upwelling phenomena. During early diagenesis, phosphatic fish debris inherit the REE patterns of the ambiant bottom water. The similar REE patterns of fish debris and the metalliferous sediments of Atlantis II Deep (LREE enrichment and positive Eu anomaly) suggest that the same process takes place between fish debris and hydrothermal fluids during sediment diagenesis [33]. All these conclusions agree quite well with the high Sm, Nd and P_2O_5 contents and low Sm/Nd ratios found for the sulphide-rich sediments of Nereus Deep core 412, and with the assumption that phosphates associated with metalliferous sediments acquired high REE contents and a specific REE pattern during the early diagenesis of the fish debris buried in the brine-impregnated sediments. REE patterns of these phosphatic phases are not controlled by the redox conditions of the sedimentary environment, but rather reflect the geochemical properties of hydrothermal fluids. The hydrothermal fluids inherited their REE pattern during reactions with neighbouring deep rocks. Feldspar dissolution could produce the observed LREE enrichments and Eu anomaly that characterize brines and metalliferous sediments [33].

Table 2
Nd isotopic compositions and Nd-Sm contents of salt-free sediments from Nereus Deep core 412. Errors represent 2σ based on within-run statistics, normalization values are given in the analytical methods section. ϵ_{Nd} was calculated following De Paolo and Wasserburg [44] using $^{143}Nd/^{144}Nd$ = 0.512638 for present-day CHUR

Sample	Depth (cm)	Nd (ppm)	Sm (ppm)	$^{147}Sm/^{144}Nd$	$^{143}Nd/^{144}Nd$	εNd
1	22-23	0.31	0.08	0.158	–	–
2	27-28	1.15	0.33	0.175	0.51300±2	*εNd= +7.1*
9	56-57	2.72	0.48	0.107	0.51258±2	*εNd= -1.2*
3	106	0.40	0.70	0.105	0.51242±2	*εNd= -4.3*
4	119	1.19	0.28	0.152	0.51271±3	*εNd= +1.4*
10	156-157	2.91	0.52	0.108	0.51262±4	*εNd= - 0.3*
5	185-186	1.68	0.22	0.083	0.51274±1	*εNd= +2.0*
6	224-225	7.70	1.37	0107	0.51284±1	*εNd= +3.9*
7	268-269	3.97	0.52	0.079	0.51279±2	*εNd= +3.0*
8	271-272	14.8	2.05	0.084	0.51260±3	*εNd= -0.7*

5.3. ϵ_{Sr} and ϵ_{Nd} values

The three groups of Nereus Deep sediments yield an inverse correlation between their ϵ_{Sr} and ϵ_{Nd} values. This is clearly expressed both on diagrams where ϵ_{Sr} and ϵ_{Nd} are plotted against depth (Fig. 4c and 4d) and on the Nd-Sr diagram (Fig. 6b). Such a correlation and the location of the metalliferous sediment field between sediments of groups A and B (Fig. 6b) is consistent with a binary mixing model for the sources of Sr

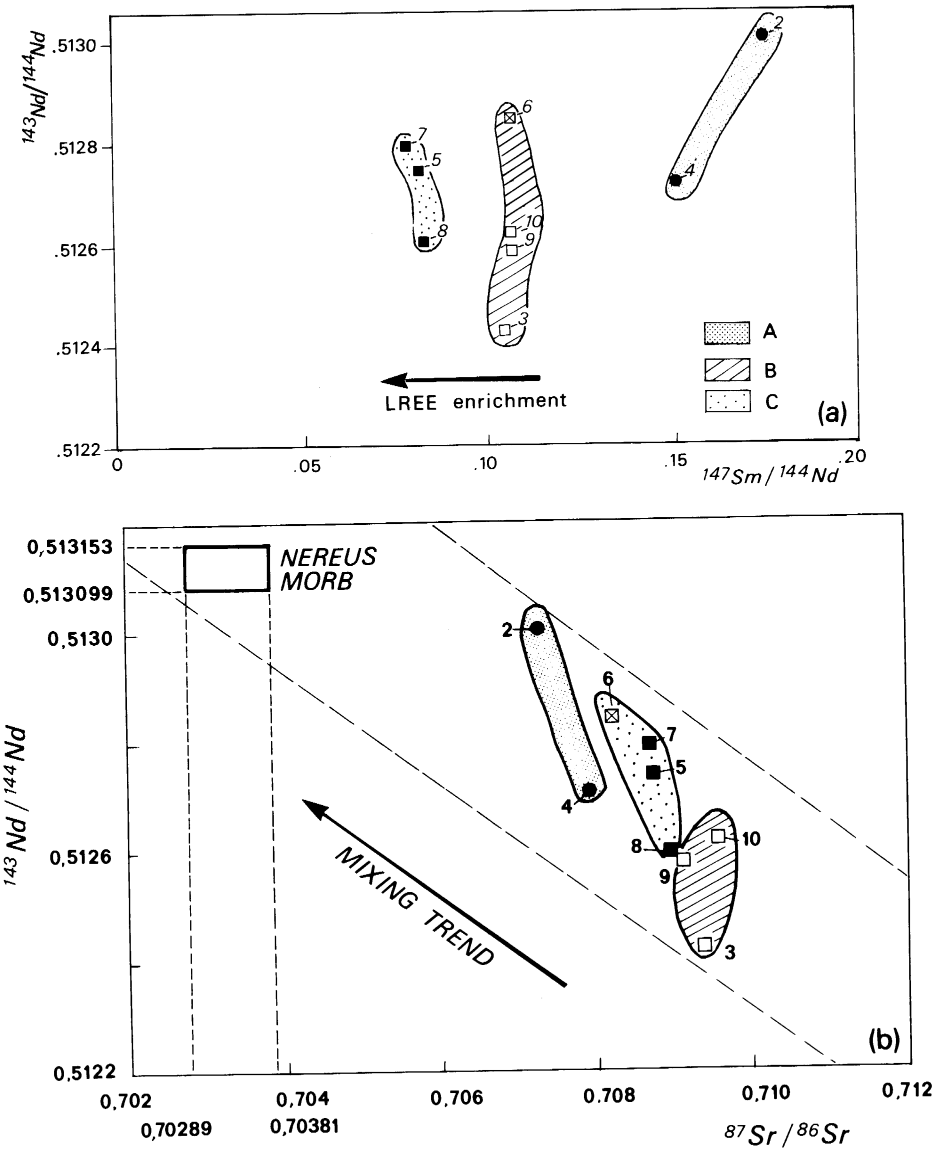

Fig. 6. (a) Plot of $^{143}Nd/^{144}Nd$ vs $^{147}Sm/^{144}Nd$ for Nereus Deep sediments, defining three fields: A = detrital samples with basaltic clasts and loose titanomagnetite crystals; B = biogenic–terrigenous sediments; C = V-rich metalliferous sediments. LREE enrichment expressed by low $^{147}Sm/^{144}Nd$ ratios characterizes sulphide-rich beds located in the lower part of the core 412 (see text). Same symbols as in Fig. 4. (b) Nd and Sr isotopic data for Nereus Deep sediments (reported Sr isotopic compositions are measured on the solid residues after the first leaching experiment). Same symbols and same fields as in (a). For comparison with Nereus Deep sediment fields A, B and C, a rectangular area encloses the data on the Nereus Deep basalts [47]. Dashed parallel lines approximately describe the limits of the binary mixing (see text). Note the intermediate location of field C (metalliferous sediments) between fields A and B (barren sediments).

and Nd in the V- and sulphide-rich sediments of core 412. In this model, Sr and Nd were derived both from sediments with basaltic clasts and loose titanomagnetite crystals (group A, high ϵ_{Nd}, low ϵ_{Sr}) and biogenic–terrigenous sediments with a continental isotopic imprint (group B, low ϵ_{Nd}, high ϵ_{Sr}). We use the Sr and Nd isotope compositions of Nereus Deep basalts [47] to define the basaltic component involved in the mixing process. On the Nd-Sr diagram (Fig. 6b), the Nereus Deep basalt field is located to the left of the sediment group A field and along the mixing trend defined by the three groups of sediments.

These three distinct types of sediments have already been recognized in different deeps of the Red Sea. In this way, on the basis of Sr and Nd isotopic data Calvez et al. [40] classified the sediments from Shaban and Atlantis II Deeps into three groups:

(1) A group of barren biogenic–terrigenous samples, found within the immature Shaban Deep and similar to sediment B of the Nereus Deep core 412.
(2) A group of metalliferous samples found in the lower part of the sedimentary pile of Atlantis II core 268. This second group shows the same Nd and Sr isotopic values as the V- and sulphide-rich sediments of the Nereus Deep.
(3) A group of sediments produced by mechanical mixing between a basaltic component and a terrigenous component, and illustrated by the sedimentary pile of Atlantis II core 198.

Located at around 26°N, where a volcanic ridge has been interpreted as being either absent or only poorly developed, the Shaban Deep only exhibits unmetalliferous sediments. Conversely, in the Atlantis II Deep, located at around 21.5°N where seafloor spreading is recognized, core 268 bears metalliferous sediments deposited at the bottom of the sedimentary pile.

5.4. *Pb isotopes*

The Pb isotope compositions and the Pb-U-Th concentrations are listed in Table 3. The analyzed

Table 3
Pb isotopic compositions and Pb-U-Th contents of salt-free sediments from Nereus Deep core 412

Sample	Depth (cm)	Pb (ppm)	U (ppm)	Th (ppm)	$^{206}Pb/^{204}Pb$	$^{207}Pb/^{204}Pb$	$^{208}Pb/^{204}Pb$
1	22-23	3.49	0.92	-	18.665 ±0.040	15.566 ±0.031	38.314 ±0.098
2	27-28	4.20	0.95	1.04	18.673 ±0.020	15.594 ±0.017	38.438 ±0.044
9	56-57	59.9	0.03	0.29	18.877 ±0.001	15.584 ±0.001	38.594 ±0.003
3	106	50.5	5.50	0.41	18.848 ±0.009	15.542 ±0.008	38.404 ±0.019
4	119	7.88	2.74	0.92	18.618 ±0.024	15.487 ±0.021	38.176 ±0.051
10	156-157	5.18	0.04	0.33	18.890 ±0.003	15.623 ±0.002	38.581 ±0.005
5	185-186	21.9	3.46	0.29	18.717 ±0.010	15.497 ±0.008	38.197 ±0.021
6	224-225	15.7	2.14	0.62	18.903 ±0.001	15.604 ±0.001	38.551 ±0.003
7	268-269	12.5	-	-	18.851 ±0.002	15.572 ±0.002	38.435 ±0.006
8	271-272	32.9	-	-	18.794 ±0.003	15.514 ±0.002	38.303 ±0.007

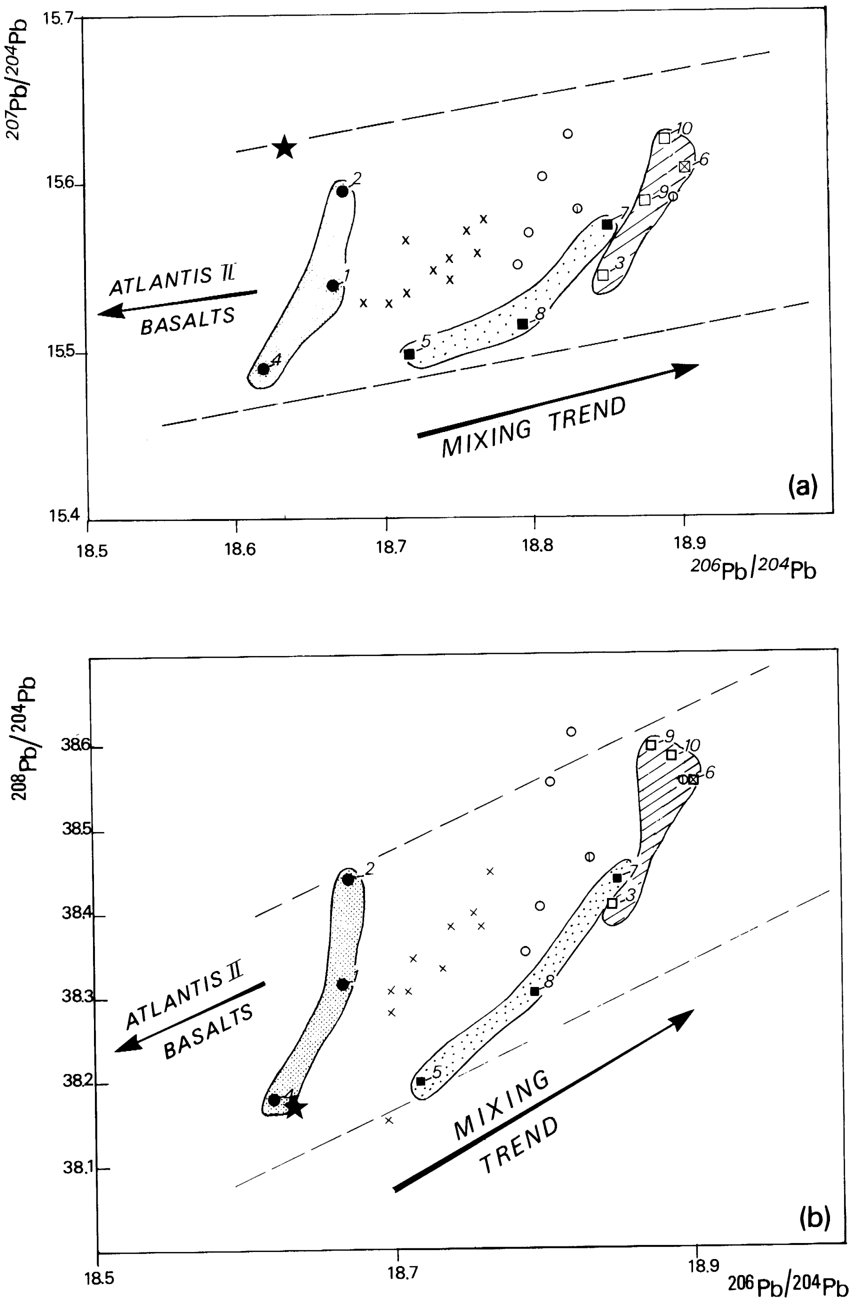

Fig. 7. $^{207}Pb/^{204}Pb$ and $^{208}Pb/^{204}Pb$ vs $^{206}Pb/^{204}Pb$ for Nereus Deep sediments (solid residues after acid leaching). Same symbols and same fields as in Fig. 6a. Dashed parallel lines approximately describe the limits of the binary mixing (see text). Again, note the location of field C (see also Fig. 6b). Also plotted for comparison are the data for a Nereus Deep basalt [52] (⋆) and for Atlantis II Deep sediments [35] including metalliferous sediments (×) and biogenic–terrigenous sediments (○). Note the similarity in the relative locations of the different sediments from the Nereus and Atlantis II Deeps, and that the unkown sedimentary end member of the mixing posited by Dupré et al. [35] to explain the Pb origin of Atlantis II metalliferous sediments could be detrital sediments with basaltic clasts and loose titanomagnetite crystals, as for the Nereus Deep.

samples have $^{206}Pb/^{204}Pb$, $^{207}Pb/^{204}Pb$ and $^{208}Pb/^{204}Pb$ ratios ranging from 18.618 to 18.903, from 15.487 to 15.603 and from 38.176 to 38.594 respectively. An important observation from the $^{206}Pb/^{204}Pb$ vs $^{207}Pb/^{204}Pb$ and $^{206}Pb/^{204}Pb$ vs $^{208}Pb/^{204}Pb$ diagrams (Figs. 7a and b) is that Nereus sediments define three separate fields, just like those previously defined on the basis of Sr and Nd isotope compositions. The $^{206}Pb/^{204}Pb$ ratios and Pb contents appear to be the best discriminating factors (Fig. 8). In good agreement with the binary mixing model suggested by Sr-Nd data, samples of group A, which are characterized by the numerous basaltic clasts, have the lowest average Pb content (5.19 ppm) and the least radiogenic $^{206}Pb/^{204}Pb$ ratios, ranging from 18.618 to 18.673. In contrast, samples of group B, which have recorded a continental imprint, present the highest average Pb content (38.52 ppm) and the most radiogenic $^{206}Pb/^{204}Pb$ ratios, ranging from 18.848 to 18.890. Finally, metalliferous V-rich samples of group C again yield intermediate values ranging between those of the two other groups, both for average Pb contents and $^{206}Pb/^{204}Pb$ ratios. A good estimate of the local basaltic component is provided by the Pb isotope composition of a Nereus MORB [52] (Figs. 7a and b). The $^{206}Pb/^{204}Pb$ and $^{208}Pb/^{204}Pb$ ratios of this basalt are similar to those of group A containing basaltic clasts, its $^{207}Pb/^{204}Pb$ value of 15.622 ± 11 being just slightly higher than those of these sediments, which range from 15.487 ± 21 to 15.594 ± 17. This variation could be explained by local Pb isotope heterogeneities in the Nereus Deep basalts, which would accord well with the Pb isotopic heterogeneïty revealed by the Red Sea basalts [53].

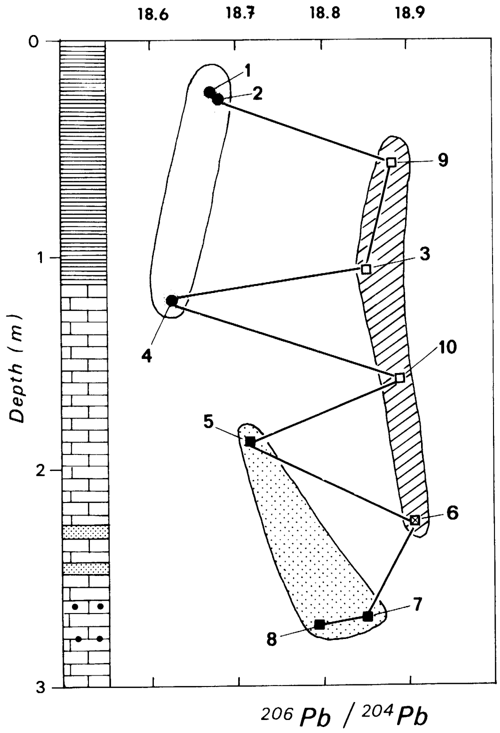

Fig. 8. $^{206}Pb/^{204}Pb$ ratios of Nereus Deep sediments (solid residues after acid leaching) versus depth (m). Same symbols as in Fig. 6a; lithology as in Fig. 3.

In conclusion, magmatic components (basaltic clasts and loose titanomagnetite crystals) of group A sediments strongly influence the Pb isotopic composition of this group. Leaching and lead extraction from such sediments by hydrothermal fluids will provide one end member of the binary mixture. Lead isotope results obtained on the 683 and 684 gravity cores in the Atlantis II Deep [35] are plotted in Figs. 7a and b in order to compare them with our results. The terrigenous sediments of the Nereus and Atlantis II Deep have very similar Pb isotope ratios, which suggest the same continental source for their detrital components. On the other hand, the Atlantis II metalliferous sediments have slightly less radiogenic $^{206}Pb/^{204}Pb$ ratios than the Nereus Deep ones, and in the same way the Atlantis II MORB show $^{206}Pb/^{204}Pb$ values ranging from 18.263 to 18.354 [35], which again are less radiogenic than the Nereus MORB values [52]. This suggests that the unknown sedimentary end member posited by Dupre et al. [35] could be similar to the A-type Nereus sediments with basaltic clasts and loose titanomagnetite crystals that were derived from the Atlantis II MORB.

5.5. Formation of the V-rich metalliferous sediments

Previous studies of oceanic sulphides from active EPR hydrothermal vents [6,54,55] have emphasized that interactions of basalt with hot hydrothermal fluids are the chief contributors to the formation of metalliferous deposits along mid-oceanic ridges. However, a Pb isotope study on metalliferous sediments from the Atlantis II Deep has suggested that the metals of these sediments are not derived from a pure basaltic source, the derivation instead involving the leaching of two sedimentary components by hot fluid circulation to explain the measured Pb isotope ratios [35]. For sedimented segments of the EPR, as in the Guyamas Basin and Escabana Trough, mixing between detrital and basaltic components has been proposed previously as a source for metals in the hydrothermal fluids and their associated sulphide deposits [7–9]. Similarly, a detailed Pb isotope study of the Troodos ophiolite [56] has outlined variations in the Pb isotope values measured for each sulphide deposit. Such isotopic heterogeneity has suggested either Pb isotope variations within the basalts that interacted with the hydrothermal fluids, or, more probably, a mixing of lead from a basaltic source and a more radiogenic component of sedimentary origin [56]. This binary mixing model suggested by the ancient sulphide deposits of the Troodos ophiolite provides a good example with which to compare the Sr, Nd and Pb isotope trends observed in the Nereus Deep sediments.

On the basis of mineralogical and chemical analyses of magnetite found in Nereus metalliferous samples, Jedwab et al. [41] suggested that basalt-derived titanomagnetites located in the upper layers of Nereus Deep core 412 were leached by hydrothermal fluids during upward percolation through the sediment. Upon cooling near the upper sediment interface, downward percolation followed and induced the growth of V-rich magnetites and sulphides in the lower part of the sedimentary pile (i.e., samples 5, 7 and 8). In good agreement with these conclusions, our Sr, Nd and Pb isotope data provide evidence of a noticeable contribution of basaltic material present as clasts or loose crystals during the V-rich metalliferous sediment formation of the Nereus Deep core. However, the Sr, Nd and Pb isotope values of the metalliferous Nereus sediments cannot be explained by a single basaltic contribution and involve a sedimentary component identified as the terrigenous detrital component expressed in samples 3, 9 and 10. This second end-member probably derives from igneous and metamorphic rocks of Precambrian or Phanerozoic age (and sedimentary rocks derived from them) exposed on the neighbouring Arabo-Nubian Shield.

Our isotope data suggest that the formation of metalliferous V-rich samples involved leaching and mixing between two main detrital components expressed in the upper part of the core. These two components were derived from the neighbouring continental crust of the Arabo-Nubian Shield and from Nereus Deep MORB.

The duality of the sources reflects the immediate vicinity of these two components in the geodynamic context of a recent oceanic rift zone. This leaching process needs a driving force, which could be found in the expulsion of fluid as a result of hydrothermal activity and its convective circulation within the sediments of Nereus Deep. The possibility of convective circulation has been tested in sediment layers in the distal part of the Bengal Fan and has been shown to be effective [57]. In this model, it is proposed that a sweeping lateral flow is superposed on a convective circulation.

In the case of Nereus Deep, the following set of events can be proposed to explain the V-rich sediment formation: In the first step (a), the upwelling hydrothermal fluid percolated through the sediments of the Nereus core, leaching the underlying sediments. During its ascent, the fluid leaches both terrigenous material types—the sediments enriched in basaltic fragments and loose titanomagnetite crystals. At a depth of less than 2 m the hot fluid was still corrosive enough to leach terrigenous and/or carbonate sediments (group B) and to continue the extraction of some elements such as Pb, Sr, Nd, Fe and V. With the fluid's temperature decreasing and its density increasing, it then began to circulate downward, describing a pattern of cell convection (stage b). At a depth of about 1.80 m the fluid cooled, this effect probably being enhanced by mixing with pore water, owing to reduced differences in density. This leads to the deposition of V-rich metalliferous layers (stage c). Thus, in this model, fluid circulation through the sediment would be responsible for the mixing of the two sources of Pb, Sr and Nd. In all the isotope diagrams (Figs. 6b, 7a, 7b and 8), sulphide-rich sediments of the bottom of Nereus Deep core 412 clearly show intermediate isotope values between those of the two sedimentary components. Experimental simulations of convective circulation in sediment layers have shown the occurrence of recurrent instabilities producing a hot upward flow related to hydrothermal expulsions. On both sides of this hot flow, cold downward flows going deep into the sediments are created [58].

On the basis of our data, the proportions of the two components leached to form the Nereus V-rich metalliferous sediments cannot be accurately defined. However, the leaching efficiency of the B sediments by a hot hydrothermal fluid is well expressed on the Pb-Pb diagrams (Figs. 7a and b) by the overlap of the respective fields of the terrigenous B sediments and the V-rich metalliferous sediments.

A single leaching process of the group A and B sediments cannot account for the Sm/Nd values of group C. Positive Eu anomalies and LREE enrichment observed in hydrothermal sediments could result from the occurrence at the sulphide levels of fish debris and/or apatites. These phosphatic phases could be considered as a third component participating in the formation of metalliferous sediments and thus modifying their REE pattern.

6. Conclusion

A systematic comparison by combining radiogenic isotope tracers remains to be done on oceanic mineralized samples occurring on sedimented and unsedimented ridges. In addition to the basaltic contribution, the involvement of sedimentary components in the metal source of oceanic sulphides and the role of sediments in the trapping of metals needs to be taken into account, these processes leading from the present oceanic ore concentrations to deposits comparable—both in grade and reserve—to ancient formations. For relating processes to tectonic location a study of discrete minerals related to fluid circulation and the subsequent chemical deposition will also be important.

Acknowledgements

We thank P. Guennoc and J. Jedwab for comments on an earlier version of the manuscript. This paper benefited greatly from the suggestions of the three anonymous reviewers. We are also grateful to J.Y. Calvez for stimulating discussion. This work was supported by non-contractual funds from the *Laboratoire de Geochronologie–Geochimie–Petrologie* (URA 1763).

References

[1] K. Borstrom and M.N.A. Peterson, The origin of aluminium-poor ferro-manganoan sediments in areas of high heat flow on the East Pacific Rise, Mar. Geol. 7, 427–447, 1969.

[2] J.B. Corliss, R.D. Ballard, J.R. Dymond, L.L. Gordon, J.M. Edmond, T.M. Van Aandel, R.R. Von Herzen and D.L. Williams, Oases of life in the Cold Abyss, Natl. Geogr., Oct. 1977.

[3] J. Francheteau, H.D. Needham, P. Choukroune, T. Juteau, M. Seguret, R.D. Ballard, P.J. Fox, W. Normak, A. Carranza, D. Cordoba, J. Guerrero, C. Rangin, H. Bougault, P. Cambon and R. Hekinian, Massive deep-sea sulphide ore deposits discovered on the East Pacific Rise, Nature 277, 523–528, 1979.

[4] J.L. Bishoff, R.J. Rosenbauer, P.J. Aruscavage, P.A. Baedecker and J.G. Crock, Sea-floor massive sulfide deposits from 21°N, East Pacific Rise, Juan de Fuca ridge and Galapagos rift: bulk chemical composition and economic implications, Econ. Geol. 78, 1711–1720, 1983.

[5] W.R. Normark, J.L. Morton, R.A. Koski, D.A. Clague and J.R. Delaney, Active hydrothermal vents and sulfide deposits on the southern Juan de Fuca ridge, Geology 11, 158–163, 1983.

[6] J. Boulegue, E.A. Perseil, M. Bernat, B. Dupre, P. Stouff and J. Francheteau, A high temperature hydrothermal deposit on the East Pacific Rise near 7°N, Earth Planet. Sci. Lett. 70, 249–259, 1984.

[7] T.K. Hinkley and M. Tatsumoto, Metals and isotopes in Juan de Fuca ridge hydrothermal fluids and their associated solid materials, J. Geophys. Res. 92, 11400–11410, 1987.

[8] J.L. Morton, M.L. Holmes and R.A. Koski, Volcanism and massive sulfide formation at a sedimented spreading center, Escabana Trough, Gorda Ridge, northeast Pacific Ocean, Geophys. Res. Lett. 14, 769–772, 1987.

[9] A.P. Le Huray, S.E. Church, R.A. Koski and R.M. Bouse, Pb isotopes in sulfides from mid-ocean ridge hydrothermal sites, Geology 16, 362–365, 1988.

[10] P.A. Rona, G. Klinkhammer, T.A. Nelsen, J.H. Treffy and H. Elderfield, Black smokers, massive sulfides and vent biota at the Mid-Atlantic Ridge, Nature 321, 33–37, 1986.

[11] P. Jean-Baptiste, J.L. Charlou, M. Stievenard, J.P. Donval, H. Bougault and C. Mevel, Helium and methane measurements in hydrothermal fluids from the mid-Atlantic ridge: the Snake Pit site at 23°N, Earth Planet. Sci. Lett. 106, 17–28, 1991.

[12] J. Honnorez, C. Mevel and B.M. Guersteen, Mineralogy and chemistry of sulfide deposits drilled from hydrothermal mount of the Snake Pit active field, M.A.R., Proc. ODP, Sci. Results 106–109, 27–45, 1990.

[13] J.E. Lupton, R.F. Weiss and H. Craig, Mantle helium in the Red Sea brines, Nature 266, 244–246, 1977.

[14] N. Blum and H. Puchelt, Sedimentary-hosted polymetallic massive sulfide deposits of the Kebrit and Shaban Deeps, Red Sea, Mineral. Deposita 26, 217–227, 1991.

[15] H. Craig, Y. Horibe, K.A. Farley, J.A. Wehlan, K.R. Kim and R.N. Henley, Hydrothermal vents in the Mariana Trough: results of the first Alvin dives, EOS 68, 477, 1987.

[16] P. Halbald, K. Nakamura, M. Wahsner, J. Lange, H. Sakai, L. Kaselitz, R.D. Hausen, M. Yamano, J. Post, B. Prause, R. Seifert, W. Michaelis, F. Teichmann, M. Kinoshita, A. Marten, J. Ishibashi, S. Czerwinski and N. Blum, Probable modern analogue of Kuroko-type massive sulphide deposits in the Okinawa Trough back-arc basin, Nature 338, 496–499, 1989.

[17] J.M. Auzende, T. Urabe, V. Bendel, C. Deplus, J.P. Eissen, D. Grimaud, P. Huchon, J. Ishibashi, M. Joshima, Y. Lagabrielle, C. Mevel, J. Naka, E. Ruellan, T. Tanaka and M. Tanahashi, In situ geological and geochemical study of an active hydrothermal site on the North Fiji Basin Ridge, Mar. Geol. 98, 259–269, 1991.

[18] Bendel, Cadre géologique et composition des minéralisations hydrothermales en contexte arriére-arc, exemple de la dorsale du bassin Nord Fidjien (Sud Ouest Pacifique), Thesis, Univ. Brest, 1993.

[19] Y. Fouquet, U. Von Stackelberg, J.L. Charlou, J.P. Donval, J. Euzinger, J.P. Foucher, P. Herzig, R. Muhe, S. Soakai, M. Wiedicke and H. Whitechurch, Hydrothermal activity and metallogenesis in the Lau back arc basin, Nature 349, 778–781, 1991.

[20] E.J. Dasch, J.R. Dymond and G.R. Heath, Isotopic analysis of metalliferous sediment from the East Pacific Rise, Earth Planet. Sci. Lett. 13, 175–180, 1971.

[21] R.K. O'Nions, S.R. Carter, R.S. Cohen, N.M. Evenson and P.J. Hamilton, Pb, Nd and Sr isotopes in oceanic ferromanganese deposits and ocean floor basalts, Nature 273, 435–438, 1978.

[22] M.L. Bender, W. Broecker, V. Gornitz, U. Middle, R. Kay, S.S. Sun and P. Biscaye, Geochemistry of three cores from the East Pacific Rise, Earth Planet. Sci. Lett. 12, 425–433, 1971.

[23] F. Albarede, A. Michard, J.F. Minster and G. Michard, $^{87}Sr/^{86}Sr$ ratios in hydrothermal waters and deposits from the East Pacific Rise at 21°N, Earth Planet. Sci. Lett. 55, 229–236, 1981.

[24] J. Bertin, J.P. Pedeux and J.C. Magenham, Contribution de la géophysique et de l'océanographie physique à la recherche et à l'exploration des boues métallifères de la Mer Rouge, in: Colloques Germinal Ressources Minérales Sous-marines, BRGM Doc. 7, 339–366, 1979.

[25] D. Bosch, Evolution géochimique initiale et précoce d'un rift: Systématique isotopique Pb, Sr et Nd du diapir mantellique de Zabargad, de son encaissant gneissique et de son hydrothermalisme: comparaison avec les sédiments métallifères et les MORB de la Mer Rouge. Conséquences géodynamiques et métallogéniques, Thesis, Univ. Montpellier II, 1990.

[26] R.G. Coleman, D.G. Hadley, R.G. Fleck, C.T. Hedge and M.M. Donato, The Miocene Tihama Asir ophiolite and its bearing on the opening of the Red Sea, in: Proc. Symp. Evolution and Mineralization of the Arabian Nubian Shield, Inst. Appl. Geol. (Jeddah) Bull. 1, 173–186, 1979.

[27] G. Feraud, V. Zumbo, A. Sebai and H. Bertrand, $^{40}Ar/^{39}Ar$ age and duration of tholeitic magmatism related to the early opening of the Red Sea rift, Geophys. Res. Lett. 18, 195–198, 1991.

[28] X. Le Pichon and J.M. Gaulier, The rotation of Arabia and the Levant fault system, Tectonophysics 153, 271–294, 1988.

[29] A.Y. Izzeldin, On the structure and evolution of the Red Sea based on geophysical data from the central and northern part, Thesis, Univ. Strasbourg, 1982.

[30] G. Pautot, P. Guennoc, A. Coutelle and N. Lyberis, Discovery of a large brine deep in the northern Red Sea, Nature 310, 133–136, 1984.

[31] C. Ramboz and M. Danis, Superheating in the Red Sea? The heat-mass balance of the Atlantis II Deep revisited, Earth Planet. Sci. Lett. 97, 190–210, 1990.

[32] Y. Thisse, Sédiments métallifères de la fosse Atlantis II (Mer Rouge): contribution à l'étude de leur contexte morphostructural et de leurs caractéristiques minéralogiques et géochimiques, Thesis, Univ. Orléans, 1982.

[33] E. Oudin and A. Cocherie, Fish debris record the hydrothermal activity in the Atlantis II deep sediments (Red Sea), Geochim. Cosmochim. Acta 52, 177–184, 1988.

[34] G. Blanc, Géochimie de la fosse Atlantis II (Mer Rouge): Evolution spatio-temporelle et rôle de l'hydrothermalisme, Thesis, Univ. Paris VII, 1987.

[35] B. Dupre, G. Blanc, J. Boulegue and C.J. Allegre, Metal remobilization at a spreading centre studied using lead isotopes, Nature 333, 165–167, 1988.

[36] W.L. Shanks and J.L. Bishoff, Ore transport and deposition in the Red Sea geothermal system: a geochemical model, Geochim. Cosmochim. Acta 41, 1507–1519, 1977.

[37] U.R. Kaplan, R.E. Sweeney and A. Nissenbaum, Sulfur isotope studies on Red Sea geothermal brines and sediments, in: Hot Brines and Recent Heavy Metal Deposits

in the Red Sea, E.T. Degens and D.A. Ross, eds., pp. 474–498, 1969.
[38] M.H. Delevaux and B.R. Doe, Preliminary report on uranium, thorium and lead contents and lead-isotopic composition in sediment samples from the Red Sea, Init. Rep. DSDP 23, 943–946, 1974.
[39] M. Shoell and W. Stahl, The carbon isotopic composition and the concentration of the dissolved anorganic carbon in the Atlantis II Deep brines/Red Sea, Earth Planet. Sci. Lett. 15, 206–211, 1972.
[40] J.Y. Calvez, A. Cocherie and E. Oudin, Sr-Nd and REE signatures of the hydrothermal activity in the Red Sea, BRGM Rep. RM10, 3 pp., 1987.
[41] J. Jedwab, G. Blanc and J. Boulegue, Vanadiferous minerals from the Nereus Deep, Red Sea, Terra Nova 1, 188–194, 1989.
[42] P. Guennoc, G. Pautot and A. Coutelle, Surficial structures of the northern Red Sea axial valley from 23°N to 28°N: time and space evolution of neo-oceanic structures, Tectonophysics 156, 1–23, 1988.
[43] P. Guennoc, G. Pautot, M.F. Le Qentrec and A. Coutelle, Structure of an early oceanic rift in the Northern Red Sea, Oceanol. Acta 13, 145–157, 1990.
[44] D. De Paolo and G.J. Wasserburg, Inferences about magma sources and mantle structure from variations of $^{143}Nd/^{144}Nd$, Geophys. Res. Lett. 3, 249–252, 1976.
[45] L. Briqueu, M. Javoy, J.R. Lancelot and M. Tatsumoto, Isotope geochemistry of recent magmatism in the Aegean arc. Sr, Nd, Hf, and O isotopic ratios in the lavas of Milos and Santorini: geodynamic implications, Earth. Planet. Sci. Lett. 80, 41–54, 1986.
[46] J.R. Lancelot and D. Bosch, A Pan-African age for the HP–HT granulite gneisses of Zabargad island: implications for the early stages of the Red Sea rifting, Earth Planet. Sci. Lett. 107, 539–549, 1991.
[47] R. Petrini, Nd-Sr isotopes on samples from the Brothers Island and Nereus Deep in the Red Sea (abstract), Terra Cognita 7, 396, 1987.
[48] A. Michard, F. Albarede, G. Michard, J.F. Minster and J.L. Charlou, Rare earth elements and uranium in high-temperature solutions from East Pacific Rise hydrothermal vent field (13°N), Nature 303, 795–797, 1983.
[49] P.N. Froelich, M.L. Bender and G.R. Heath, Phosphorus accumulation rates in metalliferous sediments on the East Pacific Rise, Earth Planet. Sci. Lett. 34, 351–359, 1977.
[50] J. Wright, R.S. Seymour and H.F. Shaw, REE and Nd isotopes in conodont apatite: variations with geological age and depositionnal environment, Geol. Soc. Am. Spec. Pap. 196, 325–340, 1984.
[51] C. Bourdillon and Y.A. Gideiri, Etude micropaléontologique de deux carottes prélevées dans la fosse Atlantis II (Mer Rouge): Age de la mise en place et milieu de dépôt des boues métallifères, C.R. Acad. Sci. Paris 296, 1271–1274, 1983.
[52] R. Altherr, F. Henjes-Kunst and A. Baumann, Asthenosphere versus lithosphere as possible sources for basaltic magmas erupted during formation of the Red Sea: constraints from Sr, Pb and Nd isotopes, Earth Planet. Sci. Lett. 96, 259–286, 1990.
[53] J.P. Eissen, T. Juteau, J.L. Joron, B. Dupre, E. Humler and A. Al'Mukhamedov, Petrology and geochemistry of basalts from the Red Sea axial rift at 18° north, J. Petrol. 30, 791–839, 1989.
[54] P. Vidal and N. Clauer, Pb, and Sr isotopic systematics of some basalts and sulfides from the East Pacific Rise at 21°N (project RITA), Earth Planet. Sci. Lett. 55, 237–246, 1981.
[55] O. Brevart, B. Dupre and C.J. Allegre, Metallogenesis at spreading centers: lead isotope systematics for sulfides, manganese-rich crust, basalts and sediments from the CYAMEX and Alvin areas (East Pacific Rise), Econ. Geol. 76, 1205–1210, 1981.
[56] B. Hamelin, B. Dupre, O. Brevart and C.J. Allegre, Metallogenesis at paleo-spreading centers: Lead isotopes in sulfides, rocks and sediments from the Troodos ophiolite (Cyprus), Chem. Geol. 68, 229–238, 1988.
[57] A. Ormond, J. Boulegue and P. Genthon, A thermo-convective interpretation of heat flow data around ODP Leg 116 in a distal part of the Bengal Fan, J. Geophys. Res., in press.
[58] P. Louvat, Geochimie et circulation convective des fluides intersticiels du rift ensedimente de Middle Valley, dorsale Juan de Fuca, Leg ODP 139, DEA Thesis, Univ. Pierre et Marie Curie, 1993.